FAILURE PREDICTION AND OPTIMAL SELECTION OF ADHESIVES FOR GLASS/STEEL ADHESIVE JOINTS

Ioannis Katsivalis[a,b,*], Ole Thybo Thomsen[c], Stefanie Feih[b] and Mithila Achintha[a]

[a] Faculty of Engineering and Physical Sciences, University of Southampton, Southampton SO17 1BJ, UK

[b] Joining Technology Group, Singapore Institute of Manufacturing Technology (SIMTech), 2 Fusionopolis Way, Singapore 138634

[c] Composites Institute (ACCIS) & Department of Aerospace Engineering, University of Bristol, Bristol BS8 1QU, UK

Mild steel/tempered glass adhesive joints are becoming a common occurrence in the construction industry. A numerical parametric study for adhesive property optimisation is conducted and determines strength and ductility as the main parameters affecting the joint performance. Numerical simulations include adhesive pressure-sensitivity, plasticity and failure modelling and are also used to further investigate onset and progression of damage leading to failure of the joints. Following this, the market of structural adhesives is scanned, resulting in the identification of an adhesive system that aligns with the 'optimal' strength and ductility parameters identified from the parametric study. The chosen adhesive system is experimentally compared and benchmarked against a brittle and a ductile adhesive in steel/glass adhesive joints subjected to four different load-cases. It is demonstrated that the proposed modelling methodology yields accurate predictions of the adhesive and adherend stress states and failure behaviour for the four different load-cases, thus highlighting the model's ability to predict the response and failure of all three adhesives and tempered glass.

Keywords: Glass structures, Glass adhesive joints, Material characterization testing, Numerical modelling

1. Introduction

The need for sustainable high performance construction materials, along with recent architectural trends and technological developments, have made glass more accessible and applicable in the construction industry [1, 2]. However, as glass is brittle, the strength of the material depends on the fracture toughness and is governed by surface flaws [2]. The brittle nature of glass also makes stress concentrations particularly undesirable for any glass structure. Stresses tend to concentrate in load introduction and connection points making the design of joints connecting glass to glass or steel to glass of utmost importance. The main connection method that is currently being used is bolted joints, which represents a durable and proven solution. However, bolted joints are structurally inefficient since holes need to be drilled in the glass surface, introducing flaws, and stress concentrations in the material, whilst the overall weight of the structure is increased [3].

An appealing alternative to bolted joints is the use of adhesively bonded joints. This method reduces stress concentrations, does not introduce discontinuities in the glass surface and does not increase overall weight significantly. Elastomers such as structural silicones are commonly being used in structural glass facades, but are generally unable to carry high shear forces in built-up glass sections due to their low strength [3]. In contrast, thermosetting polymers, like acrylics and epoxies are significantly stronger and stiffer and are currently being used extensively for bonding in load-carrying applications in other industries, for example as structural connections in composite materials [4].

Adhesive point-fixings that can be used in facades and suspended canopies have been researched previously both numerically and experimentally [5-12]. In addition, single lap joints of tempered glass connected to mild steel using different adhesives were also tested and different modelling approaches were assessed [13, 14]. Silvestru et al. [15] examined adhesive connections of laminated glass and steel under tensile and shear loading, while Machalicka and Eliasova [16] tested double lap joints connecting glass-to-glass and glass-to-metal. UV-curing acrylics were used for glass to glass connections and showed potential to be used in commercial projects [17, 18].

[*]Corresponding author
Email addresses: i.katsivalis@soton.ac.uk (I. Katsivalis), o.thomsen@bristol.ac.uk (O.T. Thomsen), feihs@simtech.a-star.edu.sg (S. Feih), Mithila.Achintha@soton.ac.uk (M. Achintha)

Most adhesives display a non-linear stress-strain response, and volume changes might take place once the plastic state is reached. Pressure-sensitive yield surface descriptions in form of the linear/exponent Drucker-Prager model were used to simulate the plastic deformations of adhesives [19]. Santarsiero et al. [10] assessed current yield/failure models being used for adhesive connections in structural glass applications and proposed a novel triaxial model which takes into account the pressure-sensitivity of the adhesives along with the non-linear effects of strain rate and temperature variation. The authors showed that the linear Drucker-Prager model is a particular case of the triaxial model they proposed. While different stress states and load conditions were tested and studied, glass failure was not considered.

Katsivalis et al. [20] performed quasi-static tensile tests on glass/steel connections via bolted, brittle (Araldite 2020) and ductile (Araldite 2047-1) adhesive joints. It was shown that bonded joints with lower strength, but ductile adhesives (in terms of bulk properties) outperformed bonded joints with stronger, but more brittle adhesives, as well as bolted joints in terms of failure load in the joint. This was explained by the development of a much larger plastic zone for the ductile adhesive within the adhesively bonded region. However, an important remaining question is how to select optimal adhesive properties for given joint geometry and loading cases by assessing the strength and ductility characteristics of an adhesive.

In this paper, tempered glass/mild steel adhesive connections are tested and analysed. Three adhesives, a brittle, high strength (Araldite 2020) [21], an intermediate strength (Delo-Duopox 03 rapid thix) [22], and a ductile (Araldite 2047-1) [23] adhesive are investigated. The joints are subjected to quasi-static loading conditions in tension, compression, in-plane and out-of-plane bending to assess the influence of different stress states. Benchmark results are also reported for bolted joints, but for brevity the paper only describes the experimental and numerical analyses relating to the adhesive joints.

This work shows that adhesives outperform bolted joints in every load case. In addition, it is shown that finite element simulations, which consider geometric non-linearity, nonlinear stress-strain adhesive characteristics, yield-surface dependent adhesive plasticity (modelled in the form of a linear Drucker-Prager model) and separate failure criteria for the glass and the adhesive can accurately predict the damage and failure of tempered glass/mild steel adhesive connections. Finally, it is highlighted that finite element analyses based studies can be successfully used to guide optimal adhesive selection and hence enhanced performance of such joints.

2. Experimental methodology

2.1 Bulk adhesive characterisation

The adhesives used in this study are Araldite 2020 which is a 2-Part, brittle, clear epoxy resin, Araldite 2047-1 which is a 2-Part ductile methacrylate and Delo-Duopox 03 rapid thix which is a 2-Part intermediate strength, clear epoxy resin. Prior to testing the double lap shear joints, the bulk properties of the adhesives were determined experimentally. More specifically, tests under uniaxial tension and compression were performed for all of the three selected adhesive material systems to characterise the elastic-plastic properties and the pressure sensitivity of the materials.

The tensile tests followed ISO 527-1:2012 and ISO 527-2:2012 [24, 25], while the compressive tests were conducted according to ISO 604:2003 [26]. The thickness of the tensile specimens according to the standards was 4 mm, while cylindrical compressive samples were used with dimensions 50 mm x 10 mm. The crosshead displacement rate, according to the standards, was set to 1 mm/min to achieve quasi-static loading conditions, and a minimum of five specimens were tested for each test. All resin bulk samples were cured for one week at ambient conditions according to manufacturer's requirements.

Instron electro-mechanical universal testing machines were used for all tests, while the strain measurements were made using strain gauges and video extensometers. Figure 1 shows characteristic specimen under uniaxial tension and compression. Figure 1 shows representative measured true stress-strain curves for the three adhesives as well as the numerical implementation utilizing the linear Drucker-Prager plasticity model, which is explained further in Section 3.

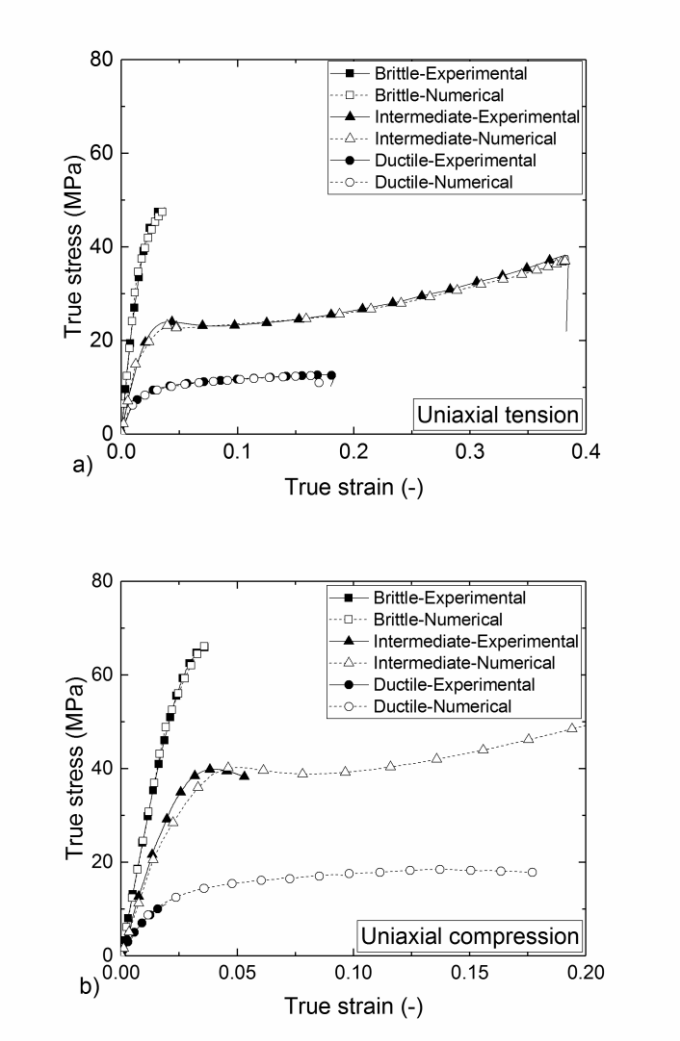

Figure 1: Representative true stress-strain curves obtained from a) tensile and b) compressive testing for the high strength, intermediate strength and ductile adhesives considered in this study.

It can be seen that the three adhesives are significantly different in terms of performance. Based on their mechanical characteristics, Araldite 2020 will be classified in this work as brittle adhesive, Delo-Duopox 03 rapid thix as intermediate strength adhesive, and Araldite 2047-1 as ductile adhesive. Table 1 summarises the key mechanical properties based on our experimental in-house testing for the three adhesives. It has to be noted that following the ISO standards it was not possible to measure the compressive strength and strain for the intermediate and the ductile adhesive due to the excessive ductility of these material systems. As a result, the tests were stopped at approximately 2-3% compressive strain. According to the standards, the modulus was derived for the strain interval between 0.05% and 0.25%, while the yield stresses and strains were derived using the 0.2% offset method.

It is worth noting that the properties measured experimentally are in agreement with the manufacturer datasheet [23] for the ductile adhesive (Araldite 2047-1) where the strength is estimated at 13-15 MPa, the strain to failure at 13-15% and the elastic modulus at 750-900 MPa, The values provided by the manufacturer for the intermediate strength adhesive (Delo-Duopox 03 rapid thix) [22] are higher for the elastic modulus (2000 MPa compared to 1540 MPa measured) and lower for the strength and strain to

failure (37 MPa compared to 33 MPa and 35% compared to 20% respectively). Finally, the datasheet of the brittle adhesive (Araldite 2020) [21] only provides value for the flexural modulus which is comparable to the tensile modulus measured (2468 MPa compared to 2570 MPa).

2.2 Adherend characteristics

The joints tested in this study consisted of tempered glass connected to mild steel splices with bolted and adhesive configurations. Tempered glass was chosen since it is typically used in glass structures where higher strength is required. In addition, designing the connections with tempered glass allowed for all different failure types to be observed (interface/substrate failures) for the different tests that were performed. The process of tempering creates compressive stresses in the glass surface, where failure typically occurs due to surface flaws. It is important to measure the residual stresses in the surface in order to estimate the strength of the glass during the experimental testing.

A scattered light polariscope (SCALP) was used to characterise the residual stress profile of the glass. The main principles of the method can be found in Aben and Guillemet [27] and Aben et al. [28], and more details on the measurement can be found in Katsivalis et al. [20]. The compressive stresses in the surface were found to exceed 100 MPa, which combined with the capacity of normal annealed glass (20-40 MPa) determine the strength of the tempered glass used in this study (120-140 MPa), assuming a superposition principle suitable for quasi-static loading conditions with a load duration not exceeding several minutes. Moisture ingress via surface flaws and glass impurities can significantly reduce these values for prolonged loading durations [1, 29], but further evaluation of the strength characteristics of glass was considered outside the scope of this paper.

For the stiffness and strength of the mild steel that was also used, standard textbook values were assumed [30]. In the analyses that follow the stresses generated in the mild steel are significantly lower than the yield/failure stresses, and therefore plasticity/failure of steel will not be considered.

2.3 Joint test set-ups

The glass-steel joints were tested for 4 different load cases. Figure 2 presents the designs of the tests conducted. The 6 mm thick glass substrates were 100 mm x 250 mm, the 6 mm thick steel splices were 110 mm x 50 mm and finally the bonded area for the adhesive joints and the contact area for the bolted joints was 50 mm x 50 mm (shaded grey in Figure 2) so that direct comparisons between the two configurations can be made. For bolted joints, the bolt hole of 10 mm was introduced at the centre of the respective adhesive joint areas. The figure also shows the location of the strain gauges used for measurement of the local strain response of the glass and steel substrates for later validation against the numerical models.

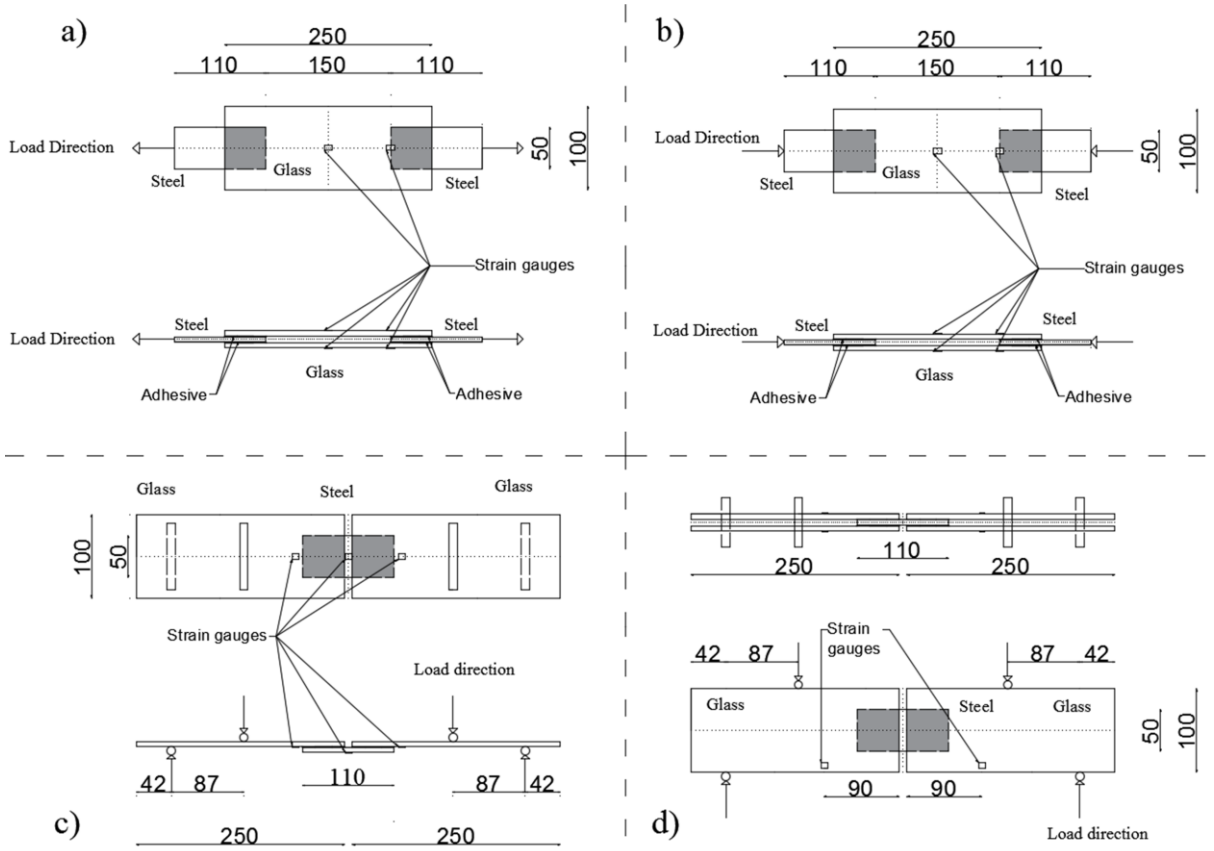

Figure 2: Design details of the a) uniaxial tension, b) uniaxial compression, c) out-of-plane bending and d) in-plane bending tests and locations of the strain gauges.

Adhesive joints were tested in 4 load cases, namely, tension, compression, out-of-plane and in-plane bending. Benchmark tests were also conducted in functionally identical bolted joints in uniaxial tension, compression and out-of-plane bending. The comparison was not performed for the in-plane bending test. The current design consists of one bolt on each side, which leads to an initially free rotation when subjected to in-plane bending. An alternative approach could be to add one bolt on each side to eliminate the free rotation, this however would also lead to a change in the size of the contact area. Therefore, the comparison with bolted joints was not conducted for this load case. A minimum of at least three specimens were tested for every load case.

For the tests in uniaxial tension and compression the loads were applied to the steel splices and transferred to the glass substrates by the adhesive joints or the bolted configurations while for the in-plane and out-of-plane bending tests, the loads were applied by steel rollers. For the in-plane bending tests an aluminium interlayer was used between the glass and the steel rollers to distribute the loads more uniformly on the glass substrates and avoid local stress concentrations resulting in premature glass fracture.

2.4 Joint manufacturing

The alignment of the joints was achieved using a steel fixture. Manufacturer recommendations for the Araldite adhesives suggest that thin adhesive layers of 0.05 to 0.1 mm lead to the greatest lap shear strength. Here, thin adhesive layers were manufactured with bondline thickness of 0.2 mm to allow repeatable manufacturing and bondline control for the given size of the joint area. For consistency, the thickness was maintained uniform for all three adhesives. It is noted that any additional thickness effect on the joint strength was not considered in this study. The thickness was controlled using 0.2 mm thick spacer wires. The manufacturing of the joints took place in a sequence of two days, since both sides of the steel splices were bonded to the glass substrates one after the other, and one day was allowed to

achieve functional strength. Afterwards, the joints were left to cure for at least one week in ambient conditions as per manufacturer recommendations.

For the bolted joints, pre-tensioned M10 bolts were used. Aluminium inserts were used to avoid direct contact of the glass substrates and the steel splices while a PTFE busing was used to avoid direct contact of the glass and the bolt. Finally, the clearance of fit was 3% and the pre-tensioning was achieved using a torque wrench and following relevant industry examples was set at 25 Nm [31].

2.5 Joint testing

The tests were conducted with an Instron 5982 testing machine with 100 kN capacity, and the loading rate of the substrates was consistently kept below 1 μstrain/sec as measured by strain gauges readings, hence ensuring quasi-static conditions throughout all the tests. Linear 120Ω strain gauges were used for the monitoring of the strains in critical locations of the joints. These locations can be identified in Figure 2 and will be explained in more detail in subsequent sections. In addition, for the measurement of the strains Vishay's Strainsmart 8000-8-SM and TML's TDS-530 systems were used.

3. Numerical simulation methodology

The numerical simulations were carried out using the commercial finite element package ABAQUS 6.14/Explicit [32]. The analyses presented in the following chapters include material and geometrical non-linearity. The steel and glass substrates are modelled as perfectly elastic materials until yield/failure. For the glass, failure is assumed to occur according to a maximum principal stress criterion; hence failure takes place once the tensile stresses exceed a certain value. This criterion is introduced in the analysis by using a brittle cracking model, a built-in ABAQUS tool [32]. According to this model, the damage initiates once a maximum stress value has been reached (varies between 120-140 MPa in this study) and then propagates based on energy-based criteria (fracture energy was 3 N/m^2 in this study [33]). However, it is known that for tempered glass complete damage can be assumed once the first crack initiates due to rapid crack propagation. The brittle cracking model has been used successfully in the past to introduce failure in annealed and tempered glass [20, 33, 34]. Steel failure does not occur and is therefore not considered in the model.

Adhesives are generally highly non-linear materials, and their plastic performance is affected by changes in both the deviatoric and the hydrostatic stress tensor [10, 19]. Due to pressure sensitivity of these materials, different levels of yield strength will be reached when the adhesive material is subjected to different stress states. For the complex multi-axial stress state usually encountered in adhesive connections, it is important to introduce models that take this sensitivity into account. According to Adams et al. [4] the yield stress in uniaxial compression is typically 1.2-1.4 times higher compared to uniaxial tension. Therefore, the linear Drucker-Prager criterion [19] was used to introduce pressure-sensitive plasticity in the adhesive layers. Equation (1) defines the linear Drucker-Prager plasticity model and Figure 3 provides a graphical representation of the yield envelope associated with the model.

$$t - p\tan\beta = d \tag{1}$$

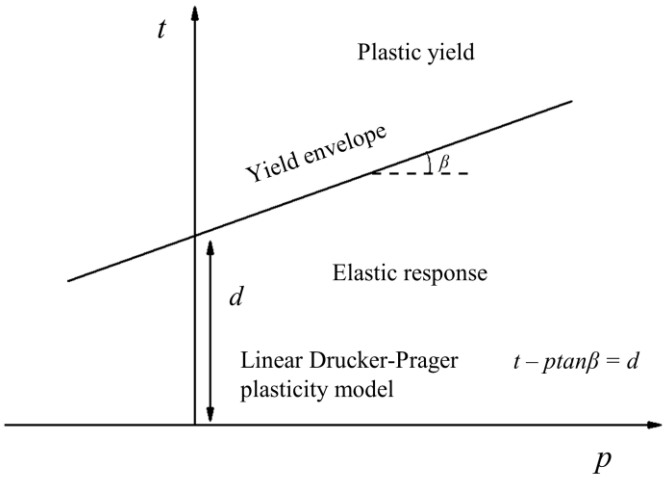

Figure 3: Graphical representation of the yield surfaces of the linear Drucker-Prager plasticity model on the meridian plane.

In equation (1), the effective stress is denoted by t and calculated from the squared difference in principal stress components $\sigma_1, \sigma_2, \sigma_3$ (eq. 2), the hydrostatic pressure stress by p (eq. 3), d is a material property related to the yield stress in pure shear (eq. 4), while the pressure sensitivity factor is introduced by $tan\beta$ (eq. 5). The parameters d and $tan\beta$ are material properties and can be defined after material characterisation testing in two stress states. In this study, tests were conducted in uniaxial tension and compression and therefore there parameters are expressed in equations (4) and (5) using the respective yield stresses σ_{yC}, σ_{yT}.

$$t = \sqrt{\frac{1}{2}[(\sigma_1 - \sigma_2)^2 + (\sigma_2 - \sigma_3)^2 + (\sigma_3 - \sigma_1)^2]} \tag{2}$$

$$p = -\frac{1}{3}(\sigma_1 + \sigma_2 + \sigma_3) \tag{3}$$

$$d = \frac{2\sigma_{yC}}{[(\sigma_{yC}/\sigma_{yT})+1]} \tag{4}$$

$$tan\beta = \frac{3[(\sigma_{YC}/\sigma_{YT})-1]}{(\sigma_{yC}/\sigma_{yT})+1} \tag{5}$$

The linear Drucker-Prager model used was calibrated numerically, and good agreement between predictions and bulk test data was achieved for the tensile and compressive stress-strain curves as shown in Figure 1. Here, the hardening curve was obtained from experimental tensile testing. Following this, the compressive test was also modelled, and values of β were varied until the best match was achieved for capturing pressure-sensitivity. For the brittle (Araldite 2020) and ductile (Araldite 2047-1) adhesives, σ_{yC}/σ_{yT} was calibrated at a value of 1.45, while for Delo-Duopox 03 rapid thix, σ_{yC}/σ_{yT} was calibrated at a value of 1.60, both higher than the 1.2-1.4 value suggested in [4].

Finally, the damage and failure in the adhesive layer was introduced by using a ductile damage failure model, a built-in ABAQUS tool [32]. According to this model, the strain at damage initiation, ε_c, depends on the stress triaxiality value. The stress triaxiality (eq. 6) is a dimensionless ratio between the hydrostatic (eq. 3) and the effective stress (eq. 2):

$$\eta = \frac{p}{t} \tag{6}$$

The strain at damage initiation, ε_c, was derived from the experimental bulk data under tension (η=1/3). The shape of the stress triaxiality-fracture strain curve was then adapted from Nguyen et al. [35]. The values of the equivalent fracture strain can be found in Table 2.

To simulate damage progression, elements of the model are removed when their stiffness has fully degraded, where at any given time step the stress tensor is described by equation (7). In equation (7), $\bar{\sigma}$ is the undamaged stress tensor, and D is the damage variable that can be attributed values between 0 and 1. The elements of the model are considered to have lost all load-carrying capacity when D=1, and are consequently deleted. The damage propagation is specified as linear softening with respect to the fracture energy of the adhesive [32]. The values of the adhesive fracture energy were calibrated on the tensile tests described in 2.1 and can also be found in Table 2.

$$\sigma = (1 - D)\bar{\sigma} \tag{7}$$

3.1 Numerical simulation of joints

The explicit solver of ABAQUS was used to take into consideration the failure models and subsequent element deletion that is required. For the models presented, semi-automatic mass scaling was introduced to reduce computational time with a stable time increment identified between 1 x 10^{-8}s to 1 x 10^{-9}s for an analysis time period of 1s. The target time step/increment was set such that the kinetic energy remained a very small fraction of the total internal energy (below 1%).

A manual edge seeding procedure was adopted to create a very dense mesh in the areas of stress concentrations, and transitioning gradually to a coarser mesh in the other parts of the model. The minimum mesh size (0.05 mm) was determined by extensive mesh sensitivity analyses, which for brevity will not be presented here. However, an example of the mesh sensitivity studies that took place can be found in Katsivalis et al. [20]. 3D stress, 8-node linear solid continuum elements with hourglass control and reduced integration (C3D8R in ABAQUS/Explicit) were used. Geometric symmetry was also used to reduce computational time and resulted in modelling one eighth of the joint for each loading configuration.

4. Results

4.1 Uniaxial loading in tension and compression

The normal and shear stress states developed in the adhesive layer during tensile and compressive loading are very similar, however the effect of the loading condition in the glass is different since glass can sustain significantly higher loads in compression than in tension. In addition, eccentricities and imperfections in the samples are exacerbated in the compressive tests and can lead to out-of-plane buckling and premature failures. However, tension and compression are stress states that are easily comparable and will therefore be presented together in this section.

As shown in Figure 2 strain gauges were applied on both sides of the joints. Two were located in symmetric locations in the midpoint of either side of the joints to capture the far field strain and possible asymmetric loading effects, while two more strain gauges were located in the areas of stress concentrations on the edges of the overlaps.

The brittle and ductile adhesive joints displayed predominantly adhesive/cohesive failure, while the intermediate strength joints failed in the glass but at significantly higher loads. All three adhesives displayed stress whitening before failure, but this was observed mostly in the ductile adhesive joints. Figure 4 shows the glass/steel surfaces after the failure of the joints. A summary for the uniaxial testing of the adhesive joints can be found in Table 3.

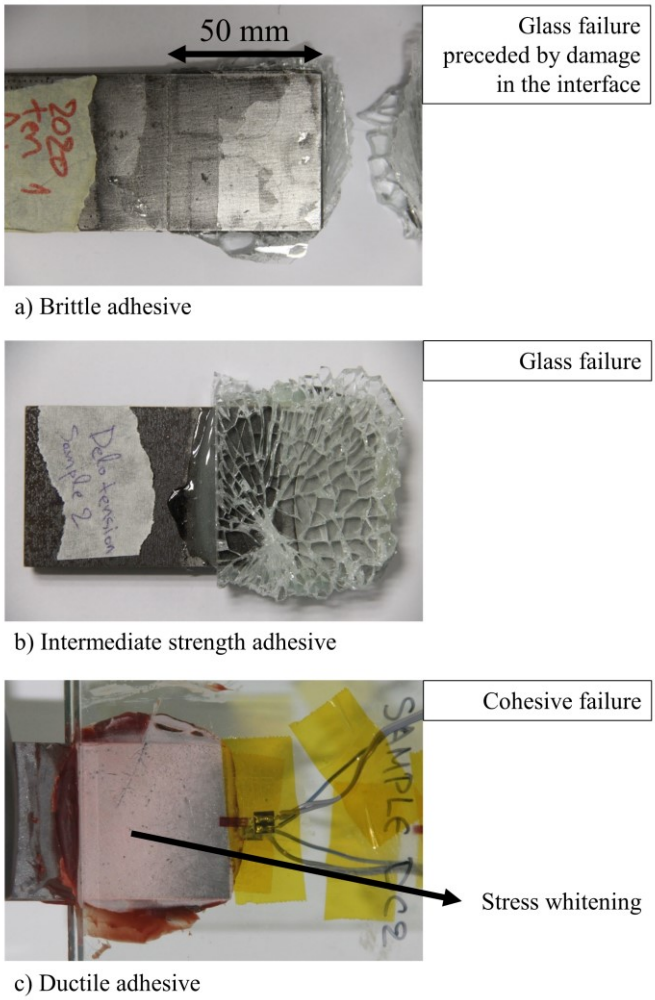

Figure 4: Typical glass/steel interfaces after failure for a) brittle, b) intermediate strength and c) ductile joints under uniaxial loading. All bonded overlap regions are 50 mm x 50 mm.

It can be seen that when subjected to tensile loading the intermediate strength adhesive outperforms (in terms of failure load) the brittle and ductile adhesive joints by 87% and 51%, respectively. For compressive loading the overall trend is the same, but the intermediate strength adhesive joint for this case outperforms the brittle and ductile adhesive joint configurations by 55% and 44%, respectively. The experimental scatter (coefficient of variation ranging from 1.5% to 16.2% for all tests) observed in the results can be explained by load and geometric eccentricities, surface flaws in the glass, and different void distributions in the adhesive layer as also reflected by the range of failure strains summarized in Table 1.

All three types of adhesive joints displayed a linear relationship between the applied load and the strain response, both in the area of the stress concentration (joint zone) and for the far field response. The linear response is explained by the fact that the strain gauges were measuring the deformation of the glass substrates. Figure 5 shows the load-strain response at the glass midpoint and the areas of stress concentration for the tensile test, while Figure 6 shows the same for the compressive test. The strain values plotted in both figures are the average between the recordings in the two substrates taken from both sides of the joint specimen.

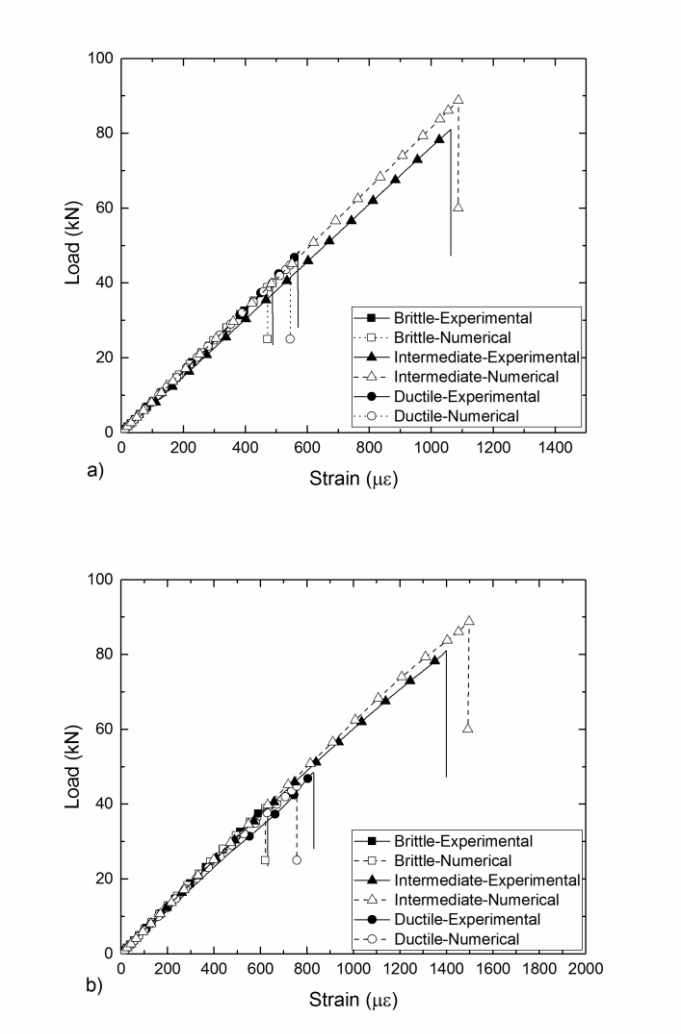

Figure 5: Comparison of load vs. strain gauge measurements and corresponding FE predictions for the joint configurations with three different adhesives subjected to tensile loading a) in the glass midpoint and b) in the areas of stress concentrations.

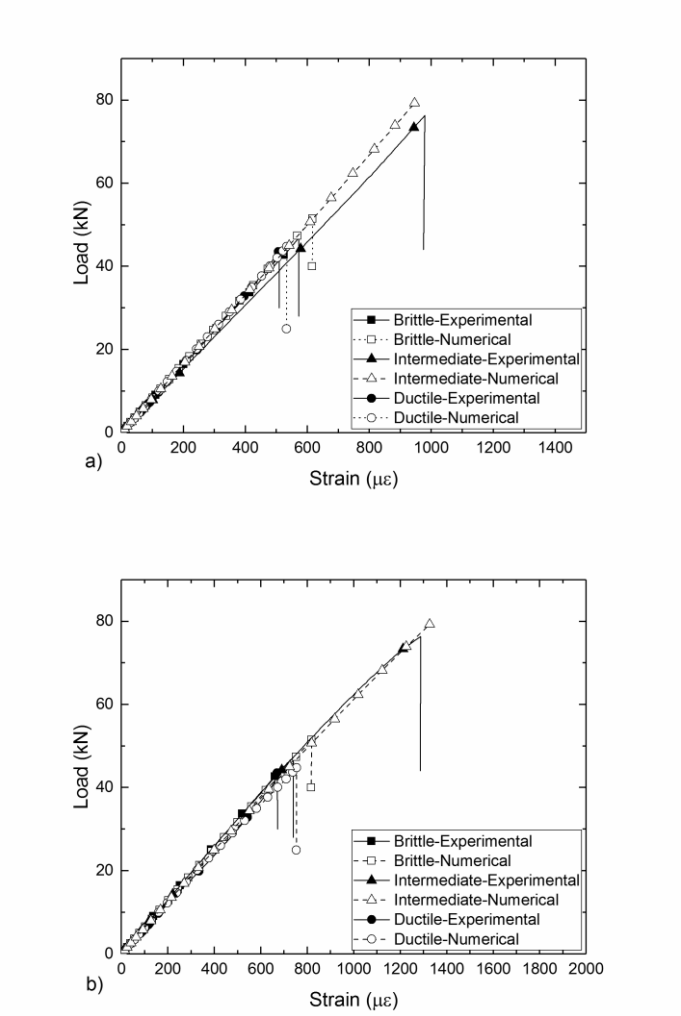

Figure 6: Comparison of load vs. strain gauge measurements and corresponding FE predictions for the joint configurations with three different adhesives subjected to compressive loading a) in the glass midpoint and b) in the areas of stress concentrations.

To provide an interpretation for the experimental scatter, a lower and an upper strength threshold was predicted through FE simulations. For the FE modelling the fracture strain of the brittle and ductile adhesives was varied based on the values of standard deviation given in of Table 1. For the case of the intermediate strength adhesive joints, failure occurs in the glass substrate and hence glass strength variation (120-140 MPa for tempered glass) determines the maximum and minimal failure load thresholds. Figure 7 plots the highest and lowest failure load as measured experimentally and predicted numerically for the joint configurations with the three different adhesives subjected to tension and compression loading.

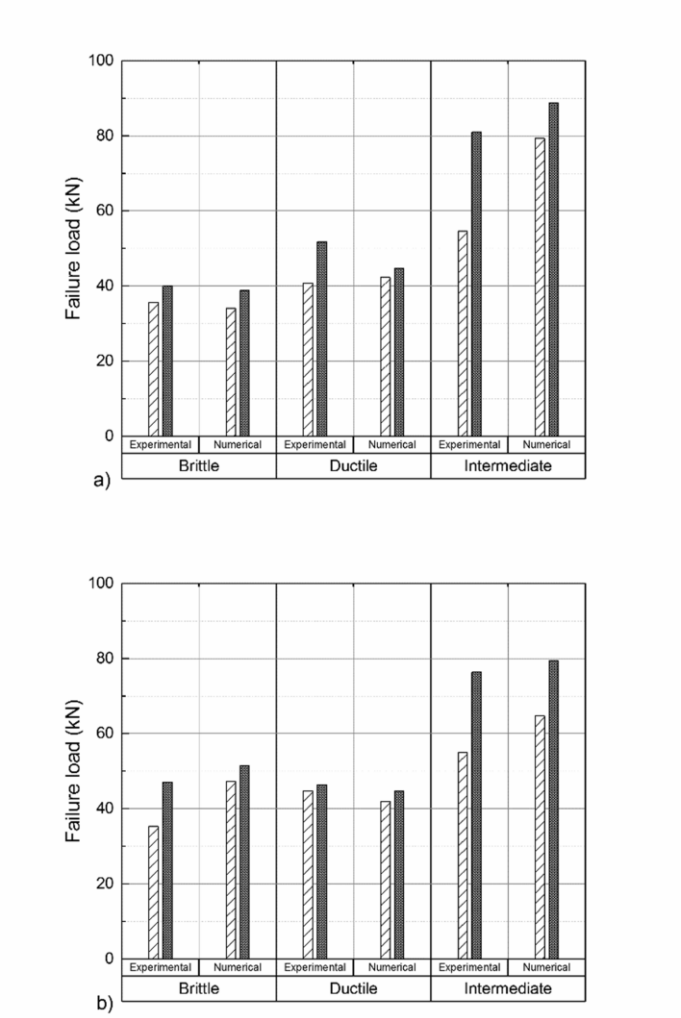

Figure 7: Summary of the failure loads as measured experimentally and predicted numerically for adhesive joints loaded under uniaxial a) tensile and b) compressive loading.

It is worth noting that for the case of compression of the intermediate adhesive strength joints, the failure load is predicted to be significantly higher than observed experimentally, assuming a perfectly straight geometry in the numerical model. The reason for this is that the FE simulations assume perfect loading distribution between the two substrates and exclude the possible occurrence of buckling. However, in the actual tests buckling was observed via strain reading bifurcations on opposite sides of the specimen, and this effect became more significant as the load was increasing. Therefore, numerical models were developed taking buckling into consideration. An initial imperfection was added in the models, following the process outlined by Feih et al [36], in the form of a small offset from the symmetry line to initiate out-of-plane buckling behaviour in the numerical simulations. The offset value was calibrated at a maximum deflection of δ=0.4 mm at the centre of the joint over a length of 370mm for the intermediate strength adhesive case. Figure 8 shows the load vs. strain response of the front and the back substrates, as measured experimentally using strain gauges and predicted numerically. It can be seen that this adjustment leads to a significantly improved prediction for the both the load-response and the failure load. The buckling effect was insignificant for the other two adhesive joint configurations due to the lower failure load.

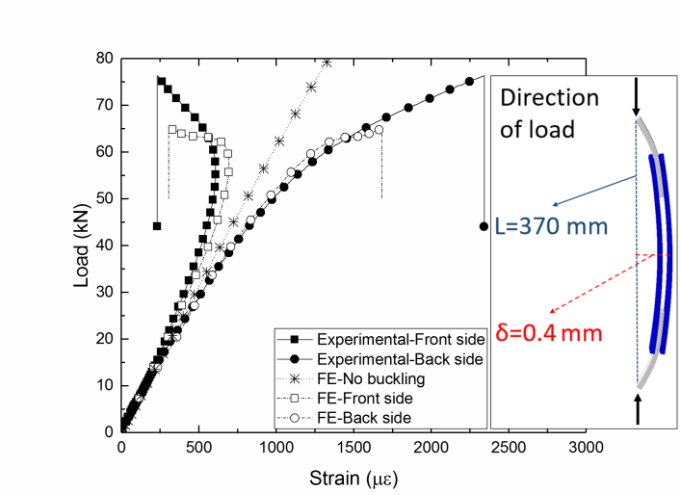

Figure 8: Load-strain response displaying buckling behaviour for the high loads achieved with the intermediate strength adhesive. The deformations indicated in the sketch to the right are exaggerated.

Summarising, the FE models were shown to provide highly accurate predictions of the load-deformation (stiffness) response for all three adhesive joint types; within 7% of the experimental observations. In addition, it was shown that the FE simulations provided failure load predictions for all three adhesives within a difference of 12% of the measured values. Additionally, upper and lower limit effects based on adhesive failure strain variations and glass strength variations agree well with the observed variations of the experimental data. Finally, for comparison, the best performing (in terms of failure load) bolted joints subjected to tension and compression loads are also included in Table 3. It can be seen that the adhesive joints are 300-800% stronger compared to a functionally identical design of bolted double shear lap joints.

4.2 Out-of-plane bending

The design of the out-of-plane bending tests and the location of the three strain gauges can be seen in Figure 2. The two strain gauges in the glass were located in symmetrical locations in the areas of stress concentration to detect any asymmetrical loading, while the third strain gauge was located on the steel substrate.

The three types of adhesive joints tested all displayed a linear strain response until failure. In terms of failure mechanism, the brittle adhesive joints displayed adhesive/cohesive failure modes, with interface failure being the predominant (about 90% of the adhesive layer failed in the interface). The ductile and intermediate strength adhesive joints failed in the glass, following stress-whitening in the adhesive.

Figure 9 shows the glass/steel interfaces after failure, and Table 4 summarises the failure loads and observed failure mechanisms for the three different joint configurations. It can be seen that the intermediate strength adhesive joints again outperform (in terms of failure load) the brittle and ductile joints by 99% and 14%, respectively. The coefficient of variation ranged from 3% for the intermediate and the ductile adhesive joints to 25% for the brittle adhesive joints. However, as mentioned earlier, the intermediate strength and ductile joints failed in the glass with only small differences in failure loads. The small difference can be explained by stress concentrations in the glass generated due to earlier damage initiation in the adhesive layer.

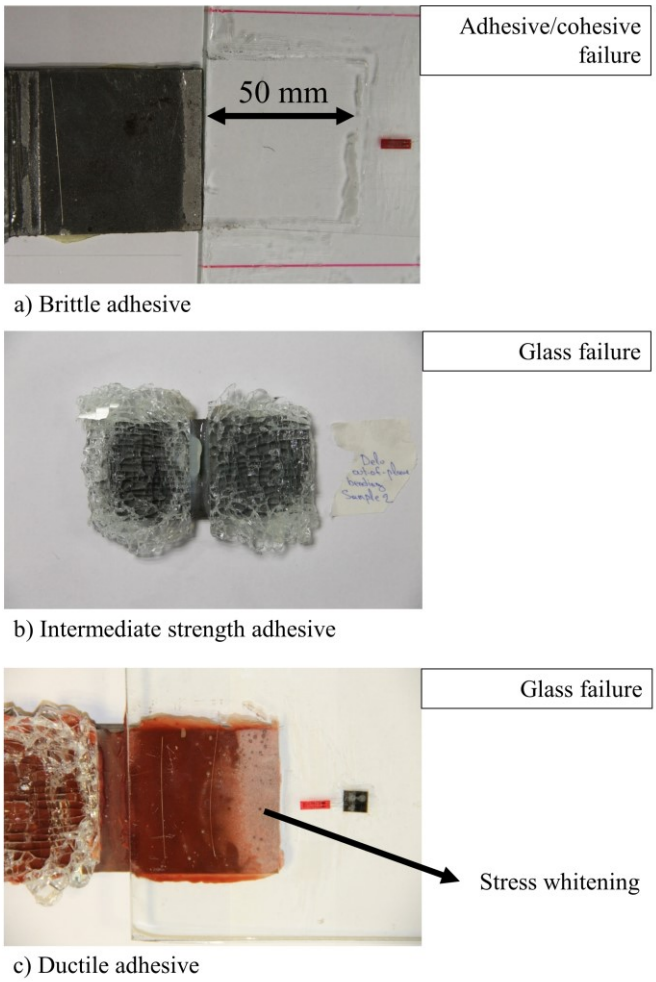

Figure 9: Typical glass/steel interfaces after failure for a) brittle, b) intermediate and c) ductile joints under out-of-plane bending loading. All bonded overlap regions are 50 mm x 50 mm.

The FE models capture accurately the strain response until failure for all three adhesives. Similarly to the uniaxial tension and compression load cases, an upper and lower limit of load predictions was possible. For the brittle adhesive, the loading limits are based on the fracture strain of the adhesive (assuming adhesive/cohesive failure), while for the ductile and intermediate strength adhesives the loading range is based on the strength limits of the glass (assuming substrate failure). Figure 10 shows the strain response in the glass and the steel as measured experimentally and predicted numerically, while Figure 11 displays the highest and lowest experimental load measurements and numerical predictions for all three types of adhesive joints.

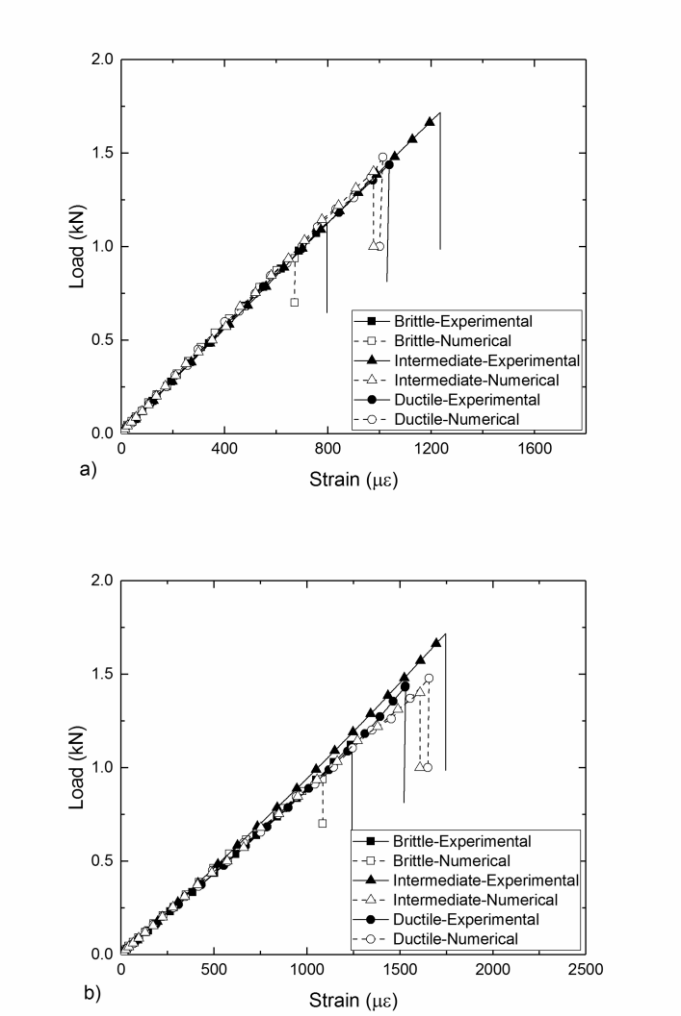

Figure 10: Comparison of strain gauge measurements and FE predictions for adhesive joints with the three different adhesives subjected to out-of-plane bending loading a) in the steel substrate, and b) the glass substrate.

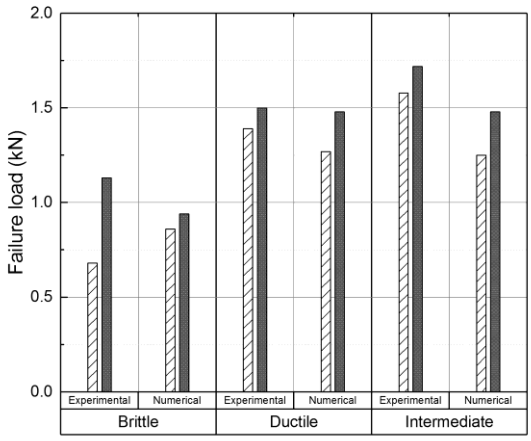

Figure 11: Summary of failure loads as measured experimentally and predicted numerically for the out-of-plane bending tests.

It can be seen that the numerical simulations accurately capture the failure mechanism and failure loads for the brittle and the ductile adhesive joints, while they slightly underestimate the failure load for the

case of the intermediate strength adhesive joints. For these joints the glass appears to fail at a slightly higher stress than the maximum stress specified numerically (~140 MPa). This is not captured by the models.

Again, the same tests were conducted for bolted joints. This is the only load-case in which the bolted joints display comparable performance with adhesive joints, and the bolted joint strength even exceeds the strength of the adhesive joint with the brittle adhesive. The percentage increase between the best performing bolted and adhesive joint is less than 30%.

4.3 In-plane bending

The design of the in-plane bending tests and the location of the strain gauges can be seen in Figure 2. For this loading condition no significant stress concentrations are expected in the vicinity of the bonded area in the glass surface, and therefore the four strain gauges were mounted in symmetrical locations on the tensile side of the four substrates. However, in this test small inaccuracies or imperfections in the glass can lead to high stress concentrations in the vicinity of the load introduction points as well as asymmetric and non-uniform load distributions. Therefore, an aluminium interlayer of 20 mm x 20 mm with 6 mm thickness was used for load spreading between the glass substrates and the steel rollers.

Linear load-strain behaviour was observed for all the tested joints with brittle and ductile adhesives, and all samples were shown to display adhesive/cohesive failure modes. More specifically, the failure in the brittle adhesive joints was about 40% cohesive while the rest was due to failure in the interface while for the ductile adhesive joints the contribution of the cohesive mode was even smaller at about 30%. For two samples of the brittle and for one sample of the ductile joints, the adhesive failure was followed by catastrophic glass failure. All the joints with intermediate strength adhesive failed in the glass before any damage was introduced in the adhesive. The failure in the glass occurred at the contact location between the glass and the aluminium interlayer in the load introduction points. Figure 12 shows the glass/steel surfaces after failure, while Table 5 summarises the failure load and mechanisms. It is worth noting that the coefficient of variation for this load-case was the lowest ranging from 1% to 5%.

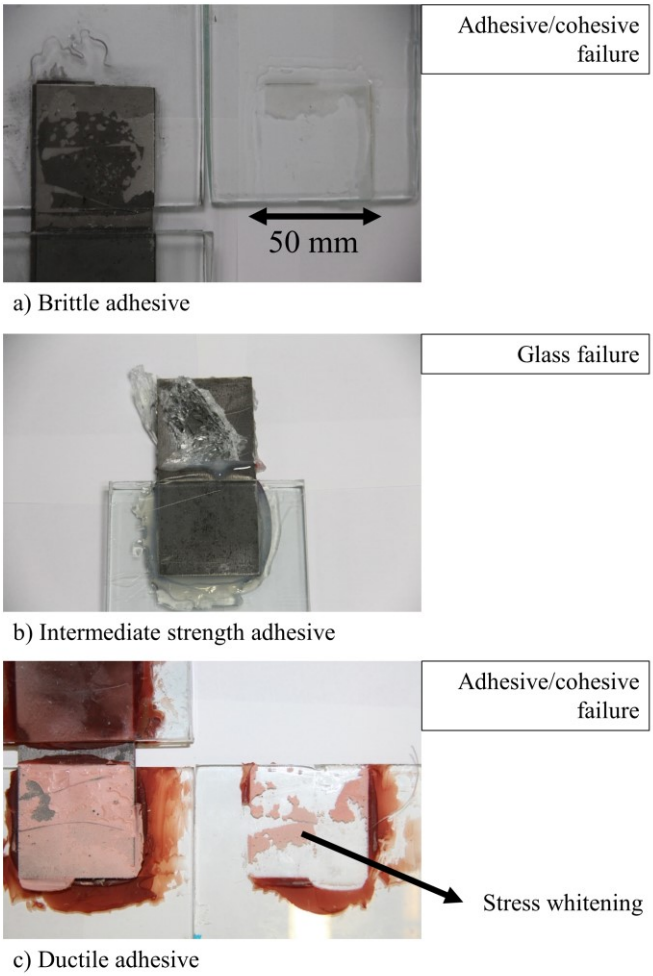

Figure 12: Typical glass/steel interfaces after failure for joints with a) brittle, b) intermediate strength and c) ductile adhesives subjected to in-plane bending loading. All bonded overlap regions are 50 mm x 50 mm.

The FE models accurately capture the strain response, failure loads and mechanisms for the joints with brittle and the ductile adhesives. Compared to the previous three load cases, the glass experiences relatively low stresses in the vicinity of the bonded area, and thus the joint failure mode characteristics depend entirely on the adhesive layer. Therefore, in this particular load case the variability of joint strength caused by the glass strength variability is removed, and this in turn leads to higher accuracy with respect to prediction of the joint strength.

For the case of joints with the intermediate strength adhesive, it is shown that joints with this adhesive outperform the joints with brittle and ductile adhesives by displaying significantly higher failure loads (82% and 30% higher, respectively). Different interlayers at the load application points could be used to reduce the stress concentrations in the contact region, but further optimisation of this test set-up is considered outside the scope of this study. It is noted that finite element analysis did not predict the glass failure at the load introduction points, most likely due to the assumptions of (a) uniformly distributed contact stresses and (b) perfectly flat surfaces in contact regions.

Figure 13 shows the strain response on the tensile side of the glass as measured experimentally and as predicted numerically, as well as the highest and lowest experimental measurements and numerical strength predictions for the three types of adhesive joints. It is seen that the failure in the joints with brittle and ductile adhesives occurs within the high/low range prediction for every joint configuration.

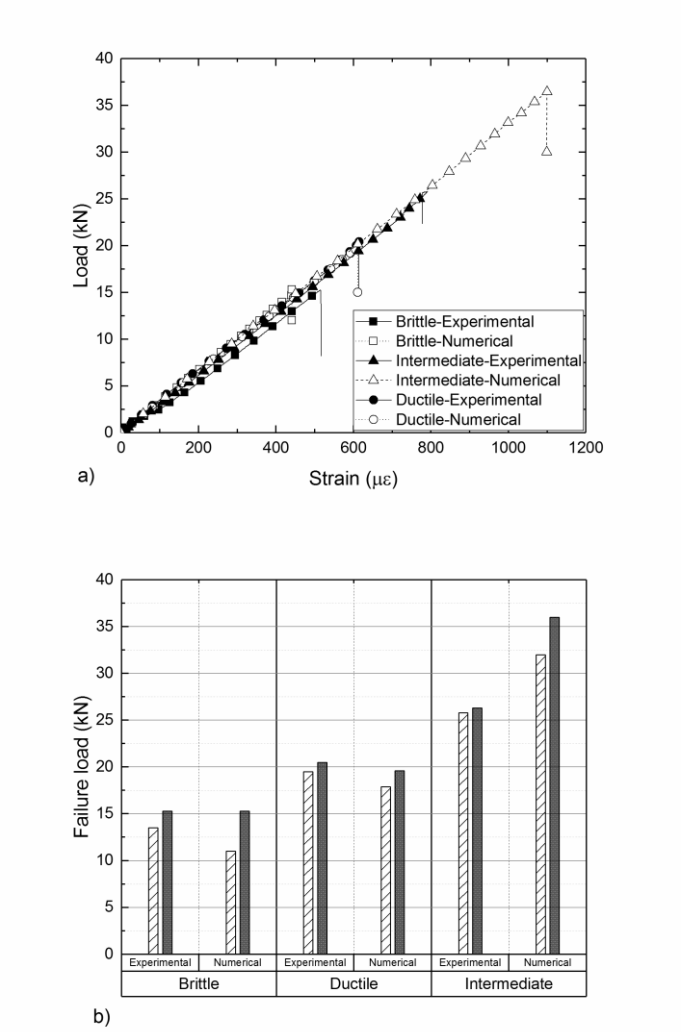

Figure 13: a) Comparison of strain gauge measurements and FE predictions for the joint configuration with the three different adhesives subjected to in-plane bending loading, and b) summary of the failure loads as measured experimentally and predicted numerically.

5. Discussion

5.1 Influence of bonded area and plastic zone development

The strongest brittle adhesive produces the weakest joints for all load cases except for the compression load case, where it displays a comparable performance (joint strength) with the joints with the ductile adhesive. This interesting and unexpected finding is investigated further in the following discussion. Figure 14 shows the predicted equivalent plastic strain distributions induced in the joints with the three different adhesive materials under tensile loading. The limited plastic region of the brittle adhesive leads to failure in the corners of the joints before the rest of the adhesive layer starts to deform plastically. Unlike the brittle adhesive, both the ductile and intermediate strength adhesives are able to develop a large plastic zone (due to their higher ductility) that extends from the corners and completely covers the 50 mm x 50 mm area of the adhesive layer. Therefore, a larger volume of adhesive material is loaded and utilised to resist the loading. This delays the failure and results in higher joint strength despite the lower strength of the adhesives. It should be noted that Figure 14 shows the deformations in the adhesive layer of a joint subjected to tensile loading, but the same observation was made for all four load-cases despite the different stress states induced in the adhesive layers for each load case.

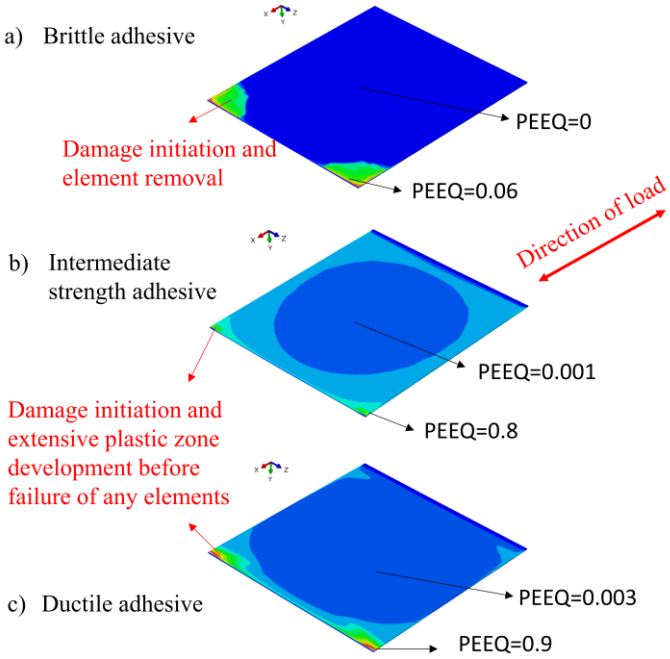

Figure 14: Equivalent plastic strain (PEEQ) distribution, plastic zone development and damage onset for tensile loading of the joint configurations with a) brittle, b) intermediate, and c) ductile adhesives. The adhesive layer size shown is 50 mm x 50 mm as per experimental test set-up.

The development of a much larger plastic zone explains why the ductile adhesive is less sensitive to the fracture strain variation compared to the brittle adhesive. A relatively small change in the adhesive failure strain, changes the failure load prediction significantly for the case of the brittle adhesive, but a bigger change has a smaller effect in the case of ductile adhesive joints.

It has to be noted however, that the plastic zone development does not only depend on the properties of the adhesive but also on the size of the bonded area. To further investigate the effect of the bonded area, a numerical parametric study with the bonded area as a varying parameter was developed. The analysis is based on the tensile test but similar results are expected in the other load-cases.

Figure 15a shows the percentage of the elements that yield in the last increment before failure for the three adhesives and Figure 15b shows the effect on the failure load of the three adhesives as the bonded area changes. It can be seen that for the intermediate and ductile adhesives, the variation of the bonded area does not have an effect on the percentage of elements that yield since the whole adhesive layer deforms plastically. However, the effect for the brittle adhesive is very important, since the percentage of elements that yield drops from about 50 % (for a bonded area of 100 mm^2) to less than 3% (for a bonded area of 2500 mm^2).

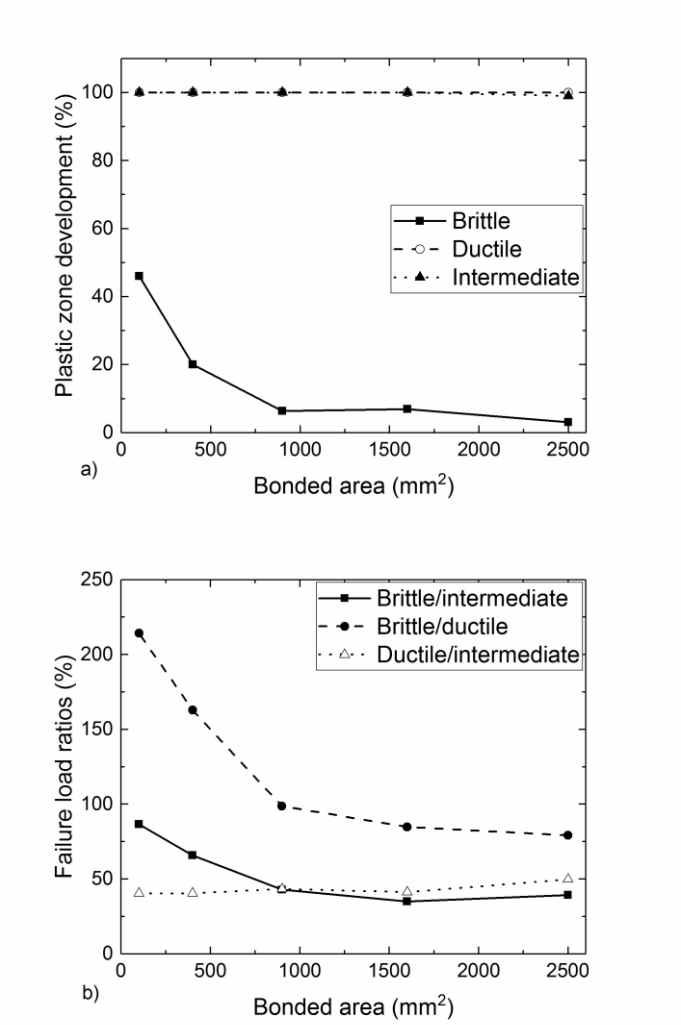

Figure 15: Effect of the size of the bonded area on a) the size of the plastic zone, and b) on the joint strength for the three different adhesives.

The size of the plastic zone though is very important when the failure load of a joint is considered. It can be seen that for smaller bonded areas when a significant amount of the brittle adhesive layer yields, the brittle adhesive outperforms the ductile adhesive and has comparable performance to the intermediate strength adhesive. As the joints' size increases however, the plastic zone develops in a smaller part of the joint, and therefore the performance of the brittle adhesive starts to deteriorate compared to the other two adhesives.

5.2 Optimal adhesive selection

The numerical analyses show that the joint strength is governed by the mechanical properties of the adhesives used. The main adhesive material properties are strength and strain-to-failure, but the adhesive stiffness and fracture toughness are also important. The detailed study conducted included three adhesive systems, with the intermediate adhesive generally performing best, but it is unclear whether even higher performing adhesive systems are available in the market. To enable more general conclusions about the optimal adhesive selection for the presented joint geometries and load cases included in this study, the market for structural adhesives was surveyed thoroughly.

A range of adhesives with different property characteristics resulting in an upper bound curve were chosen for a parametric study to determine the maximum failure load as a function of strength and fracture strain. The adhesives selected range from stiff and strong adhesives to flexible and ductile, and their mechanical properties are summarized in Table 6 as established from manufacturers' data sheets [22, 37-42]. The graphs in Figure 16 demonstrate the general trends for commercially available adhesives based on this upper bound selection: (1) with increasing strength the strain-to-failure reduces (Figure 16a), (2) strength increases and strain-to-failure decreases with an increase in stiffness (Figure 16b) and (3) fracture toughness increases with strain-to-failure and decreases with strength (Figure 16c). Nonlinear trend-lines as per best data fit were plotted for all three graphs to visualize these relationships.

Joint strength simulations were conducted for all data points shown in Figure 16. Figure 17 shows the distribution of the predicted joint failure loads, assuming simplified perfect elastic-plastic behaviour and standard values for pressure-sensitivity. It is worth noting that the strength of the joints is governed by stress concentrations on the corners of the overlaps. These concentrations depend on both the strength/ductility of the adhesives but also on their stiffness. It is observed that a peak of the predicted failure load occurs around an adhesive strength value of 30 MPa and an adhesive strain to failure of ca. 23%. The presence of such distinctive joint strength peaks suggests that an optimal choice of adhesive exists for the considered joint configuration and tensile load case.

Finally, it is noted that these 'optimal' adhesive properties are most closely associated with the adhesive system 'Delo-Duopox 03 rapid thix', which is the best performing adhesive in the experimental part of this study for all load cases investigated. Accordingly, this adhesive selection strategy reveals that this particular resin system can indeed be considered an optimal choice for the considered load cases. It should be noted that a similar approach can be utilized as an initial screening test for any type of joint geometry and loading condition.

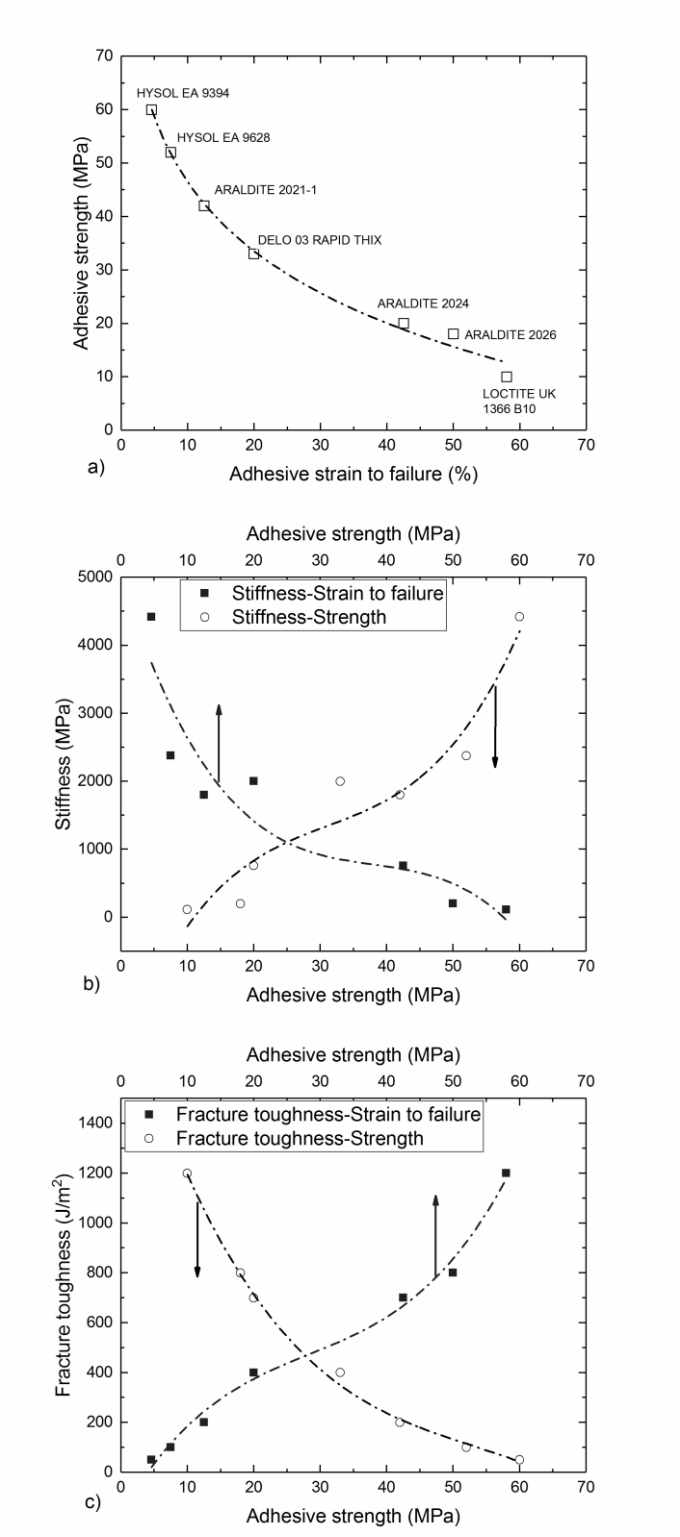

Figure 16: Correlation of a) adhesive strength vs strain to failure, b) adhesive strength and strain to failure vs stiffness, and c) adhesive strength and strain to failure vs fracture toughness for common structural adhesives. Data from various manufacturers' datasheet [22, 37-42].

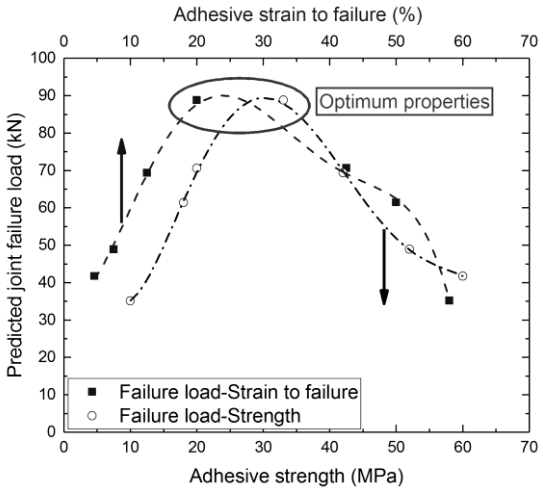

Figure 17: Correlation of the predicted tensile failure load of bonded joints with the strength/strain of the adhesives found in Figure 16.

6. Conclusions

A combined experimental and numerical study of the load response and failure behaviour of glass adhesive joints is presented in this paper. An experimental test campaign was carried out to distinguish between the performance of a brittle, an intermediate strength and a ductile adhesive used in bonded joints subjected to four different loading scenarios that connections encounter in glass structures; namely tension, compression, in-plane and out-of-plane bending. In addition to being compared against each other in terms of resulting joint strength, the adhesive joint behaviour was also compared with the failure loads obtained for reference bolted joints.

The experimental study has shown that the joints with an intermediate strength adhesive system outperformed all other joints for every load case. However, it has to be noted that the failure mechanism switched from a predominantly adhesive/cohesive mode to failure in the glass.

It is also important to note that all the tested types of adhesive joints displayed higher strength than bolted joints under quasi-static loading. The only load case in which bolted joints displayed comparable strength was for out-of-plane bending where the joints failed at higher loads than observed for the brittle adhesive, and slightly lower joint strength than achieved for the joints with intermediate strength and ductile adhesives. No comparative assessment was made between bolted and adhesive joints for the in-plane load case due to the free rotation that would be induced in the bolted joints. Finally, it was found that for every loading scenario bolted joints failed catastrophically in the glass substrate, while a variety of different failure mechanisms were observed for the bonded joints.

Considering numerical modelling, the authors previously showed [20] that the combination of a linear Drucker-Prager model with a ductile damage failure model for the adhesive, and a brittle cracking model for glass can accurately predict the load response and failure behaviour of glass adhesive joints subjected to tensile loading. It was shown in this paper that the methodology developed in [20] is generally applicable and that it can be expanded and adapted to other load-cases. Additionally, for compression loading, it is important to consider the effects of small initial geometric distortions leading to out-of-plane movement for high strength joints. It is finally noted that the ductile damage model is very sensitive, especially when brittle adhesives are considered, to the strain to failure assumed in the model, and therefore the reliability and accuracy of the material characterisation can exert significant effect on the accuracy of the model predictions.

In addition, the failure mechanisms associated with the three different adhesives were studied, and it has been shown that adhesive ductility plays a critical role. Unlike the brittle adhesive, the intermediate

strength and the ductile adhesives develop an extended plastic zone, which redistributes the loads and suppresses or reduces the effect of local stress concentrations. However, the plastic zone development and hence the strength of the joint, does not only depend on the properties of the adhesive but also on the geometry of the joint. It has been shown that adhesive strength is more important for smaller size joints, while the ductility becomes more critical as the bonded area increases in size.

Based on these observations, a numerical parametric study was conducted to screen commercial adhesive systems systematically. The study showed that for the joint designs and geometrical configurations examined, adhesives that combine intermediate values of strength and ductility produce stronger bonded joints. The experimental test campaign conducted as part of the research presented in this paper confirms this conclusion and further validates the capability of the nonlinear FE analyses for joint design and optimisation.

Finally, it is important to note that all tests and analyses were limited to static loading in ideal laboratory conditions. Cyclic loading, humidity and temperature variation will be present in actual engineering structures, and this needs to be considered before safe conclusions regarding the use of adhesive joints in building structures can be drawn. In such cases the exposure, number of loading cycles, their duration and the surface preparation is expected to play a much more significant role and this is an important topic of future research.

Acknowledgements The principal author gratefully acknowledges the funding from the Agency for Science, Technology and Research (A*STAR), Singapore, and the University of Southampton, UK, that has enabled the conduction of the research reported.

References

1. Achintha, M., *5 - Sustainability of glass in construction*, in *Sustainability of Construction Materials (Second Edition)*, J.M. Khatib, Editor. 2016, Woodhead Publishing. p. 79-104.

2. IStructE, *Structural use of glass in buildings*. Second edition. ed. 2014, London: Institution of Structural Engineers, SETO.

3. Haldimann, M., A. Luible and M. Overend, *Structural use of glass*. Structural engineering documents ;. 2008, Zürich, Switzerland: International Association for Bridge and Structural Engineering. 215 p.

4. Adams, R.D., J. Comyn and W.C. Wake, *Structural adhesive joints in engineering*. 2nd ed. 1997, London: Chapman & Hall. x, 359 p.

5. Dispersyn, J., S. Hertelé, W.D. Waele and J. Belis, *Assessment of hyperelastic material models for the application of adhesive point-fixings between glass and metal.* International Journal of Adhesion and Adhesives, 2017. **77**: p. 102-117.

6. Dispersyn, J. and J. Belis, *Numerical research on stiff adhesive point-fixings between glass and metal under uniaxial load.* Glass Structures & Engineering, 2016.

7. Dispersyn, J., J. Belis and J. De Jaegher, *Influence of corner and edge distance of adhesive point-fixings for glass structures.* Engineering Structures, 2015. **105**: p. 174-185.

8. Dispersyn, J., M. Santarsiero, J. Belis and C. Louter, *A preliminary study of the nonlinearity of adhesive point-fixings in structural glass facades.* Journal of Facade Design and Engineering, 2014. **2**: p. 85-107.

9. Van Lancker, B., J. Dispersyn, W. De Corte and J. Belis, *Durability of adhesive glass-metal connections for structural applications.* Engineering Structures, 2016. **126**: p. 237-251.

10. Santarsiero, M., C. Louter and A. Nussbaumer, *A novel triaxial failure model for adhesive connections in structural glass applications.* Engineering Structures, 2018. **166**: p. 195-211.

11. Santarsiero, M., C. Louter and A. Nussbaumer, *Laminated connections under tensile load at different temperatures and strain rates.* International Journal of Adhesion and Adhesives, 2017. **79**: p. 23-49.

12. Santarsiero, M., C. Louter and A. Nussbaumer, *Laminated connections for structural glass applications under shear loading at different temperatures and strain rates.* Construction and Building Materials, 2016. **128**: p. 214-237.

13. Nhamoinesu, S. and M. Overend, *The Mechanical Performance of Adhesives for a Steel-Glass Composite Facade System*, in *Challenging Glass 3*. 2012. p. 293-306.

14. Overend, M., S. Nhamoinesu and J. Watson, *Structural Performance of Bolted Connections and Adhesively Bonded Joints in Glass Structures.* Journal of Structural Engineering, 2013. **139**(12): p. 04013015.

15. Silvestru, V.A., M. Drass, O. Englhardt and J. Schneider, *Performance of a structural acrylic adhesive for linear glass-metal connections under shear and tensile loading.* International Journal of Adhesion and Adhesives, 2018. **85**: p. 322-336.

16. Machalicka, K. and M. Eliasova, *Adhesive joints in glass structures: effects of various materials in the connection, thickness of the adhesive layer, and ageing.* International Journal of Adhesion and Adhesives, 2017. **72**: p. 10-22.

17. Weller, B., F. Nicklisch, V. Prautzsch and I. Vogt, *Outline of Testing and Evaluation Program Used in Selection of Adhesives for Transparent Adhesive Joints in All-Glass Load-Bearing Structures.* Journal of ASTM International, 2012. **9**(4): p. 1-17.

18. Oikonomopoulou, F., T. Bristogianni, F.A. Veer and R. Nijsse, *The construction of the Crystal Houses façade: challenges and innovations.* Glass Structures & Engineering, 2018. **3**(1): p. 87-108.

19. Dean, G., L. Crocker, B. Read and L. Wright, *Prediction of deformation and failure of rubber-toughened adhesive joints.* International Journal of Adhesion and Adhesives, 2004. **24**(4): p. 295-306.

20. Katsivalis, I., O.T. Thomsen, S. Feih and M. Achintha, *Strength evaluation and failure prediction of bolted and adhesive glass/steel joints.* Glass Structures & Engineering, 2018. **3**(2): p. 183-196.

21. Huntsman, *Araldite 2020 (XW 396 / XW 397) - Technical Data Sheet*. 2007: Basel.

22. Delo Industrial Adhesives, *Delo-Duopox 03 rapid thix - Technical Data Sheet*. 2018, Delo Industrial Adhesives: Windach.

23. Huntsman, *Araldite 2047-1 -Technical Data Sheet*. 2010: Basel.

24. ISO, *ISO 527-1:2012, Plastics – Determination of tensile properties, Part 1: General principles*. 2012, International Organization for Standarization.

25. ISO, *ISO 527-2:2012, Plastics – Determination of tensile properties, Part 2: Test conditions for moulding and extrusion plastics*. 2012, International Organization for Standarization.

26. ISO, *ISO 604:2002, Plastics – Determination of compressive properties*. 2002, International Organization for Standarization.

27. Aben, H. and C. Guillemet, *Photoelasticity of glass*. 1993, Berlin ; London: Springer-Verlag.

28. Aben, H., J. Anton and A. Errapart, *Modern photoelasticity for residual stress measurement in glass.* Strain, 2008. **44**(1): p. 40-48.

29. Ciccotti, M., *Stress-corrosion mechanisms in silicate glasses.* Journal of Physics D: Applied Physics, 2009. **42**(21): p. 214006.

30. Oberg, E. and C.J. McCauley, *Machinery's handbook : a reference book for the mechanical engineer, designer, manufacturing engineer, draftsman, toolmaker, and machinist*. 29th ed. ed. 2012, New York: Industrial Press.

31. IStructE, *Structural use of glass in buildings*. 1999, London: Institution of Structural Engineers, SETO. 168p.

32. Simulia, D.S., *ABAQUS 6.14*. 2014: Providence, RI, USA.

33. Bedon, C. and M. Santarsiero, *Laminated glass beams with thick embedded connections – Numerical analysis of full-scale specimens during cracking regime.* Composite Structures, 2018. **195**: p. 308-324.

34. Bedon, C., K. Machalická, M. Eliášová and M. Vokáč, *Numerical Modelling of Adhesive Connections Including Cohesive Damage.* Challenging Glass Conference Proceedings, 2018: p. 309-320%V 6.

35. Nguyen, A.T.T., N. Pichitdej, M. Brandt, S. Feih and A.C. Orifici, *Failure modelling and characterisation for pin-reinforced metal-composite joints.* Composite Structures, 2018. **188**: p. 185-196.

36. Feih, S., E. Kandare, B.Y. Lattimer and A.P. Mouritz, *Structural Analysis of Compression Deformation and Failure of Aluminum in Fire.* Journal of Structural Engineering-Asce, 2011. **137**(7): p. 728-738.

37. Loctite, *LOCTITE EA 9394 AERO - Technical Data Sheet*. 2013.

38. Loctite, *LOCTITE EA 9628 AERO - Technical Data Sheet*. 2013.

39. Loctite, *LOCTITE UK 1366 B10 / LOCTITE UK 5452 - Technical Data Sheet*. 2014.

40. Huntsman, *Araldite 2024 (XD 4666 A/B) - Technical Data Sheet*. 2004: Duxform, Cambridge.

41. Huntsman, *Araldite 2026 - Technical Data Sheet*. 2011: Basel.

42. Huntsman, *Araldite 2021-1 Technical Datasheet*. 2016: Basel.

Tables

Table 1: Summary of measured properties for the Araldite 2020, Araldite 2047-1, and Delo-Duopox 03 rapid thix adhesive systems

	Brittle Adhesive (Araldite 2020)	**Ductile Adhesive (Araldite 2047-1)**	**Intermediate strength adhesive (Delo-Duopox 03 rapid thix)**
Resin system	Epoxy	Methacrylate	Epoxy
Young's modulus (*E*), GPa *	2.57 ± 0.08	0.89 ± 0.08	1.54 ± 0.23
Poisson's ratio (ν) *	0.38 ± 0.004	0.42 ± 0.001	0.4 ± 0.002
Tensile yield strength (σ_{yT}), MPa *	31.33 ± 2.73	5.56 ± 0.11	13.52 ± 2.22
Compressive yield strength (σ_{yC}), MPa **	56.76 ± 5.01	6.75 ± 0.45	22.46 ± 2.53
Tensile failure stress (σ_{fT}), MPa *	45.39 ± 2.61	13.10 ± 1.13	37.20 ± 3.40
Compressive failure stress (σ_{fC}), MPa **	65.66 ± 0.4	-	-
Tensile failure strain (ε_{fT}), % *	3.1 ± 0.6	17 ± 4.1	35.6 ± 4.5
Compressive failure strain (ε_{fC}), % **	3.5 ± 0.3	-	-
Pressure sensitivity factor (*tanb*)	0.55	0.55	0.69

* ISO 527-1:2012 and ISO 527-2:2012 [24, 25]
** ISO 604:2003 [26]

Table 2: Damage model material parameters

	Brittle Adhesive (Araldite 2020)	**Ductile Adhesive (Araldite 2047-1)**	**Intermediate strength adhesive (Delo-Duopox 03 rapid thix)**
Fracture energy, (J/m^2)	100	700	400
Stress triaxiality (η)	**Fracture strain (ε_c)**		
-0.33	0.186	1.31	3.67
0	0.01	0.077	0.21
0.33	0.019	0.131	0.367
0.5	0.027	0.162	0.551
0.75	0.015	0.104	0.294

Table 3: Summary of the failure loads/mechanisms for the adhesive joints tested subjected to uniaxial tension and compression loads.

Type of joint	**Tension**		**Compression**	
	Measured failure load [kN]	**Failure mechanism**	**Measured failure load [kN]**	**Failure mechanism**
Brittle Adhesive (Araldite 2020)	38.0 ± 1.8	Significant damage in the adhesive layer/interface leading to glass failure	42.4 ± 5.1	Significant damage in the adhesive layer/interface leading to glass failure
Ductile Adhesive (Araldite 2047-1)	47.0 ± 4.6	Cohesive failure	45.5 ± 0.7	Cohesive failure
Intermediate strength adhesive (Delo-Duopox 03 rapid thix)	71.0 ± 11.5	Glass failure	65.5 ± 8.7	Glass failure, preceded by buckling of the joints
Bolted	8.0 ± 0.7	Glass failure	9.7 ± 3	Glass failure

Table 4: Summary of the failure loads and observed failure mechanisms for the adhesive joints tested subjected to out-of-plane bending.

Type of joint	**Measured failure load [kN]**	**Failure mechanism**
Brittle Adhesive (Araldite 2020)	0.83 ± 0.21	Adhesive (90-100%) /cohesive failure (0-10%)
Ductile Adhesive (Araldite 2047-1)	1.45 ± 0.04	Glass failure
Intermediate strength adhesive (Delo-Duopox 03 rapid thix)	1.65 ± 0.05	Glass failure
Bolted	1.20 ± 0.08	Glass failure

Table 5: Summary of the failure load and mechanisms for the adhesive joints tested under in-plane bending.

Type of joint	Measured failure load [kN]	Failure mechanism
Brittle Adhesive (Araldite 2020)	14.3 ± 0.7	1) Adhesive (60%-70%) /cohesive failure (30%-40%) 2)Glass failure preceded by significant damage in the adhesive layer
Ductile Adhesive (Araldite 2047-1)	20.0 ± 0.4	1) Adhesive (70%-80%) /cohesive failure (20%-30%) 2) Glass failure preceded by significant damage in the adhesive layer
Intermediate strength adhesive (Delo-Duopox 03 rapid thix)	26.0 ± 0.2	Premature failure in the glass for all joints due to the contact at the load introduction points
Bolted	N/A	This configuration is not applicable to bolted joints since it leads to free rotation

Table 6: Mechanical properties of adhesives selected for the optimal screening selection. Data from various manufacturers' datasheet [22, 37-42].

Adhesive	Young's modulus (E), MPa	Tensile failure stress (σ_{fT}), MPa	Tensile failure strain (ε_{fT}), %	Fracture energy, J/m^2	Predicted failure load, kN
Hysol EA 9394	4420	60	4.6	50	41.8
Hysol EA 9628	2377	52	7.5	100	49
Loctite 5452	114	10	58	1200	25.2
Delo-Duopox 03 rapid thix	2000	33	20	400	88.8
Araldite 2024	760	20	42.5	700	70.6
Araldite 2026	200	18	50	800	61.5
Araldite 2021-1	1800	42	12.5	200	69.4

Figure captions

Figure 1: Representative true stress-strain curves obtained from a) tensile and b) compressive testing for the high strength, intermediate strength and ductile adhesives considered in this study.

Figure 2: Design details of the a) uniaxial tension, b) uniaxial compression, c) out-of-plane bending and d) in-plane bending tests and locations of the strain gauges.

Figure 3: Graphical representation of the yield surfaces of the linear Drucker-Prager plasticity model on the meridian plane.

Figure 4: Typical glass/steel interfaces after failure for a) brittle, b) intermediate strength and c) ductile joints under uniaxial loading. All bonded overlap regions are 50 mm x 50 mm.

Figure 5: Comparison of load vs. strain gauge measurements and corresponding FE predictions for the joint configurations with three different adhesives subjected to tensile loading a) in the glass midpoint and b) in the areas of stress concentrations.

Figure 6: Comparison of load vs. strain gauge measurements and corresponding FE predictions for the joint configurations with three different adhesives subjected to compressive loading a) in the glass midpoint and b) in the areas of stress concentrations.

Figure 7: Summary of the failure loads as measured experimentally and predicted numerically for adhesive joints loaded under uniaxial a) tensile and b) compressive loading.

Figure 8: Load-strain response displaying buckling behaviour for the high loads achieved with the intermediate strength adhesive. The deformations indicated in the sketch to the right are exaggerated.

Figure 9: Typical glass/steel interfaces after failure for a) brittle, b) intermediate and c) ductile joints under out-of-plane bending loading. All bonded overlap regions are 50 mm x 50 mm.

Figure 10: Comparison of strain gauge measurements and FE predictions for adhesive joints with the three different adhesives subjected to out-of-plane bending loading a) in the steel substrate, and b) the glass substrate.

Figure 11: Summary of failure loads as measured experimentally and predicted numerically for the out-of-plane bending tests.

Figure 12: Typical glass/steel interfaces after failure for joints with a) brittle, b) intermediate strength and c) ductile adhesives subjected to in-plane bending loading. All bonded overlap regions are 50 mm x 50 mm.

Figure 13: a) Comparison of strain gauge measurements and FE predictions for the joint configuration with the three different adhesives subjected to in-plane bending loading, and b) summary of the failure loads as measured experimentally and predicted numerically.

Figure 14: Equivalent plastic strain (PEEQ) distribution, plastic zone development and damage onset for the joint configurations with a) brittle, b) intermediate, and c) ductile adhesives. The adhesive layer size is 50 mm x 50 mm.

Figure 15: Effect of the size of the bonded area on a) the size of the plastic zone, and b) on the joint strength for the three different adhesives.

Figure 16: Correlation of a) adhesive strength vs strain to failure, b) adhesive strength and strain to failure vs stiffness, and c) adhesive strength and strain to failure vs fracture toughness for common structural adhesives. Data from various manufacturers datasheet [22, 37-42].

Figure 17: Correlation of the predicted tensile failure load of bonded joints with the strength/strain of the adhesives found in Figure 16.